Improving the performance of an RF resonant cavity water-cut meter using an impedance matching network

Heron Eduardo de Lima Ávila[a,b], Daniel J. Pagano[b], Fernando Rangel de Sousa[a]

[a]*Department of Electrical Engineering*
[b]*Department of Automation and Systems*
Federal University of Santa Catarina
88040-900 Florianópolis, Brazil
heron.eduardo.avila@gmail.com, daniel.pagano@ufsc.br, fernando.rangel@eel.ufsc.br

Abstract

In multiphase flow measurement, one of the most challenging issues is to define an adequate technology for a specific scenario, taking into account the measurement accuracy, implementation feasibility and costs. The electromagnetic technology based on resonant cavities are often employed in water-cut meters to measure two-phase flows such as water/oil and water/gas mixtures. The main disadvantage of this technology is the electromagnetic signal attenuation that occurs as the water content decreases. This undesirable behavior is amplified due to the impedance mismatch between the sensor ports and the transmitter/receiver modules. This paper presents a study to implement an impedance matching network in order to improve the instrument performance. Impedance matching networks were built, taking into account the matching for a 100%, 50% and, also, for the worst case of 0% of water fraction where there is a hardly signal attenuation. The implemented networks improved the signal amplitude ratio between the first resonant mode and the other modes, increasing the identification accuracy of the first resonance peak.

Keywords: impedance matching, resonant cavity sensor, two-phase flow, radio frequency, water-cut meter

1. Introduction

In almost all stages of the petroleum production, there are multiphase flows, such as water/oil/gas, or water/oil and water/gas mixtures. In order to evaluate the productivity of an oil field, it is important to monitor how much water, oil, and gas is being produced. Several technologies have been developed in order to estimate the relative quantities in a multiphase flow flowing in an oil pipe, such as electrical capacitance tomography [1], fiber optic reflectometer [2], ultrasound [3], and electromagnetic waves [4], [5], [6], [7]. Sensors that employ electromagnetic technology, such as resonant cavity sensors, are based on dielectric properties of the multiphase flow in the RF and microwave frequency range [8], [9], [5]. They are usually used in flows containing water, due to the large difference between the electric permittivity of the water ($\varepsilon_{relative} \approx 81$ for frequencies bellow 1 GHz) and those of other flows, such as oil ($\varepsilon_{relative} \approx 2$).

The electromagnetic technology, based on resonant cavities employed in water-cut meters to measure two-phase flows, is the main issue of this paper. In this tech-nology, the resonant frequency of the sensor depends on the effective permittivity of the multiphase flow inside the pipeline. By measuring the transmission coefficient of the sensor as a function of the frequency, we determine the frequency where the resonance occurs. This information is then processed in order to find a correspondence with a given multiphase flow pattern, which was previously established in a characterization procedure.

In order to measure the transmission coefficient, it is often employed a 50 ohms-based RF network analyzer. The accuracy of the measurement is strongly related to the signal-to-noise ratio at the receiver input, which is very dependent on the quality of the impedance matching at the instrument ports. Moreover, the port impedance of the sensor changes with the flow pattern. Thus, in order to minimize the reflections on the ports and consequently maximize the amplitude ratio between the first and the others signal peaks, the use of impedance matching networks is imperative to enhance the measurement accuracy. The problem of signal attenuation was also reported in an acoustic two-phase

flow measurement system [10], where the amplitude ratio of the RF signal exponentially decreases as the gas flow rate increases. In [11], the problem of the instability on the resonance frequency measurement due to the increasing of the gas mass fraction was investigated. The two last references do not take into account the impedance matching approach.

The passive impedance matching networks are often used to maximize the power transfer between two devices. Several matching techniques have been employed in different applications, such as in communications systems, wireless power transfer, medicine, etc. [12], [13], [14], [15]. A particular characteristic of the proposed water-cut meter is that the impedance of the ports varies according to the water content inside the cavity, thus an adaptative matching network should be employed in order to provide a complete solution.

In this paper, we present a study regarding the adoption of an impedance matching network to improve the measurement characteristic of a water-cut resonant cavity sensor. The proposed measurement system operates in the frequency range from 150 MHz to 300 MHz. Inside this frequency operating range, three impedance matching networks were implemented to match the impedance between the transmitter/receiver modules and the sensor RF antennas. In this sense, three different cases 0%, 50% and 100% of water fraction were evaluated, since it is enough to validate the proposed method.

It is noteworthy that the impedance matching method proposed in this paper improve remarkably the detection of the first resonant peak of the sensor response. This is the main contribution of this paper.

The paper is organized as follows. The working principle of the sensor and how its signal degrades with changes in the pipeline water fraction content are shown in Section 2. Section 3 presents the proposed impedance matching design through a circuit-level analysis. Simulation and experimental results are explained in Section 4. Finally, some conclusions are drawn in Section 5.

2. Working principle

Resonant cavities are closed metallic devices made in a rectangular or cylindrical shape, in which the energy is stored in the electromagnetic fields at a high frequency. The resonance occurs at the frequency in which the excitation field will be in phase with the reflection components, resulting in a high standing wave pattern inside the cavity. This phenomenon occurs at distinct frequencies corresponding to different propagation modes, denoted by: Transversal Electric TE_{nml} and Transversal

Magnetic TM_{nml}, where n, m, and l, refer to a maximum electric field at a wave pattern in the cavity directions [8]. The resonance frequency of a cylindrical cavity can be determined by [8]

$$f_{r,nml} = \frac{1}{2\sqrt{\mu\varepsilon}}\left[\left(\frac{p_{nm}}{\pi a}\right)^2 + \left(\frac{l}{d}\right)^2\right]^{1/2},\qquad(1)$$

where p_{nm} are mth-order Bessel functions of the first kind, that vary according to the propagation mode; a is the cavity radius and d is the cavity length; μ is the permeability of the material defined as $\mu = \mu_0\mu_r$, where μ_0 is the magnetic permeability of free space and μ_r is the relative permeability; ε is the electric permittivity of the material, being $\varepsilon = \varepsilon_0\varepsilon_r$, where ε_0 is the permittivity of free space, and ε_r is the relative permittivity. The relative permittivity ε_r is a complex value, usually represented by $\varepsilon_r = \varepsilon_r' + j\varepsilon_r''$, where the imaginary part stands for the losses of the material.

The sensor was built, as depicted in Fig. 1(a), using a 3 inches in diameter PVC pipe inside another 5 inches in diameter metallic pipe, both of them with 5.9 inches in length. The cavity was designed to resonate around 300 MHz for the TE111 resonant mode. A sketch and a photograph of the implemented sensor prototype are shown in Fig. 1(a) and 1(b), respectively. Replacing the sensor parameter values in (1) we can find the resonance frequency as

$$f_{r,TE111} = \frac{kc}{\sqrt{\varepsilon_m}}\qquad(2)$$

where $k = 5.69$ is a constant, c is the speed of the light in vacuum and ε_m is the relative permittivity of the mixture inside the sensor. Note that from Eq. 2, the resonant frequency of the cavity sensor is inversely proportional to the square root of the material's permittivity and that the permittivity varies with the fraction of water inside the cavity. This is the physical principle of the proposed water-cut meter.

The probe antennas are positioned on the metallic cavity wall where the electric field is maximum. The sensor response depends on the position of the antennas (vertical or horizontal, see fig. 2). In a horizontal way the response curve of the sensor (resonant frequency versus water fraction) becomes more linear than in a vertical way. This result can be investigated by the resonant cavity perturbation method [16], [8], [17], [18].

The resonant cavity perturbation method is useful to measure the material dielectric properties. In the material perturbation method, the material sample is inserted

(a)

(b)
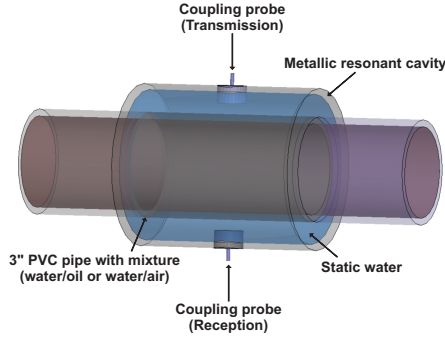
Figure 1: Sketch (a) and photograph (b) of the resonant cavity sensor.

(a)

(b)

Figure 2: Electric field distribution inside the resonant cavity for TE111 propagation mode according to the antennas placement (a) horizontal (tangential to the sample surface) and (b) vertical (normal to the sample surface).

into the cavity, and so the resonant frequency and quality factor are measured.

A resonant cavity with volume V and partially filled with a material whose volume is V_s, is characterized by means of the relative permittivity (ε_{r1}) and the relative permeability (μ_{r1}). The cavity designed to resonate at a specific resonant mode presents an electric field $\bar{\mathbf{E}}_1$ and a magnetic field $\bar{\mathbf{H}}_1$ at the resonance frequency ω_1. The electromagnetic fields ($\bar{\mathbf{E}}_2$ and $\bar{\mathbf{H}}_2$) together with the resonance frequency $\omega_2 = \omega_1 + \Delta\omega$ are modified when a perturbation of the permittivity $\Delta\varepsilon_r = \varepsilon_{r2} - \varepsilon_{r1}$ and permeability $\Delta\mu_r = \mu_{r2} - \mu_{r1}$ is induced in the material sample. The general formula of the perturbation method, taking into account perfect conductive cavity walls and a small perturbation, is given by [8]

$$\frac{\omega_2 - \omega_1}{\omega_2} = \frac{\int_{V_s}[(\varepsilon_{r2}\varepsilon_{r1})\varepsilon_o\bar{\mathbf{E}}_2\bar{\mathbf{E}}_1^* + (\mu_{r2} - \mu_{r1})\mu_o\bar{\mathbf{H}}_2\bar{\mathbf{H}}_1^*]dV}{\int_V[\varepsilon_{r1}\varepsilon_o\bar{\mathbf{E}}_2\bar{\mathbf{E}}_1^* + \mu_{r1}\mu_o\bar{\mathbf{H}}_2\bar{\mathbf{H}}_1^*]dV},$$

$$(3)$$

where the indexes 1 and 2 represent the results before and after the insertion of the sample into the cavity.

Assuming that the original medium in the cavity is lossless and considering a small and homogeneous volume fraction of the material sample inside the cav-

ity, with large permittivity and constant permeability ($\mu_{r2} = \mu_{r1}$), the general formula (3) can be rewritten as

$$\frac{\omega_2 - \omega_1}{\omega_2} \approx -\frac{\int_{V_s}(\varepsilon_{r2} - \varepsilon_{r1})\bar{\mathbf{E}}_2\bar{\mathbf{E}}_1^*dV}{2\varepsilon_{r1}\int_V \bar{\mathbf{E}}_2\bar{\mathbf{E}}_1^*dV}.$$

$$(4)$$

For the TE111 propagation mode employed in the proposed sensor, when the antennas are placed at horizontal position (see Figure 2(a)), the electric field inside the cavity becomes tangential to the sample surface. In that case the electric field inside the sample equals to the electric field outside the cavity ($E_2 = E_1 = E$) such that the equation (4) can be rewritten as

$$\frac{\Delta f_r}{f_r} \approx -\frac{S}{2}\left(\frac{\varepsilon_{r1}'(\varepsilon_{r2}' - \varepsilon_{r1}') + \varepsilon_{r1}''(\varepsilon_{r2}'' - \varepsilon_{r1}'')}{(\varepsilon_{r1}')^2 + (\varepsilon_{r1}'')^2}\right) = A_hS \quad (5)$$

where S stands for the "filling factor" that is the relation between the integral of the electric fields inside the sample volume V_s and the integral of the electric fields of whole cavity volume V.

When the antennas are placed at vertical position (see Figure 2(b)), the electric field inside the cavity becomes

3

normal to the sample surface. In this case the electric field inside the sample becomes $E_i = E_e/\varepsilon_r$, and equation (4) can be rewritten as

$$\frac{\Delta f_r}{f_r} \approx -\frac{S}{2} \left(\frac{\varepsilon'_{r2}(\varepsilon'_{r2} - \varepsilon'_{r1}) + \varepsilon''_{r2}(\varepsilon''_{r2} + \varepsilon''_{r1})}{(\varepsilon'_{r2})^2 + (\varepsilon''_{r2})^2} \right) = A_v S. \quad (6)$$

The antenna placement analysis was done taking into account experimental measurements, varying the water fraction inside the sensor pipe from 10% to 100%. Experimental data acquisition was made using a transmitter (Signal Hound USB-TG44A) and a receiver (Signal Hound USB-SA44B) modules both from Test Equipment Plus. The transmitter and receiver modules were configured to operate as a Scalar Network Analyzer (SNA), powered and controlled by a computer connected to the modules by a USB cable, and configured to perform a frequency sweep from 100 MHz to 400 MHz with 500 kHz step size. The electrical connection between the antennas (Tx and Rx) was made through 50 ohms coaxial cables. A beaker scale was used to measure the amounts of water. A block diagram and a real picture of the implemented setup is shown in Figure 3. We consider that f_{r1} is the resonance frequency with 0% of water, whereas f_{r2} is the resonance frequency after the sample insertion, and a volume fraction varying from 10% to 100% of water.

Isolating ε_m in (2) we can see that there are different values for the real part of the relative permittivity after the sample insertion in the cavity. We also consider that ε_{r1} is the relative permittivity for 0% of water fraction, whereas ε_{r2} is the relative permittivity from 10% to 100% of water fraction. In a pure state, fresh water present null conductivity, and in the range from 100 MHz to 400 MHz the imaginary part of the relative permittivity is approximately 1, although in nature there are minerals dissolved in water that affect the permittivity values [8], [19]. Therefore, in our analysis, we consider that $\varepsilon''_{r1} \approx \varepsilon''_{r2} = 1$, and in that case, equations (5) and (6) can be rewritten as following:

$$\frac{\Delta f_r}{f_r} \approx -\frac{S}{2} \left(\frac{\varepsilon'_{r2} - \varepsilon'_{r1}}{\varepsilon'_{r1}} \right) = A'_h S, \quad (7)$$

$$\frac{\Delta f_r}{f_r} \approx -\frac{S}{2} \left(\frac{\varepsilon'_{r2} - \varepsilon'_{r1}}{\varepsilon'_{r2}} \right) = A'_v S. \quad (8)$$

From the former assumptions, we compute the frequency shift $\Delta f_r/f_r$ curves as shown in Figure 4. As we
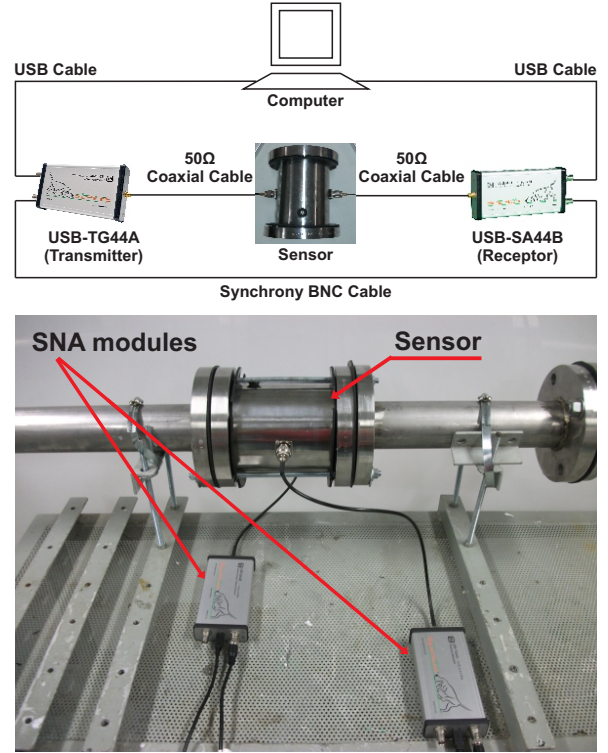
Figure 3: Block diagram and real picture of the implemented setup.

can see through the Figure 4, the measurements from the horizontal antennas placement (Figure 4(a)) have a more linear characteristic curve than those from the vertical antennas placement (Figure 4(b)). Therefore, we conclude that the electric field distribution injected in a horizontal way, will present better results than the vertical configuration. According with this analysis, for the remainder of this document, all the measurements were made taking into account the horizontal antenna configuration of the sensor.

The magnitude of the transmission coefficient S_{21} of the sensor, when the water fraction decreases from 100% to 0% in a stratified water/air mixture, is shown in Figure 5. The amplitude ratio between the first and the others peaks, gradually increases and below 50% of water, the first resonance peak almost disappears. This signal attenuation occurs mainly due to (i) the water content decreases and (ii) it is amplified by the impedance mismatch between the sensor ports and the transmitter/receiver modules. Clearly, there is an impedance mismatch in the studied sensor as we will see in detail in Section 3.

4
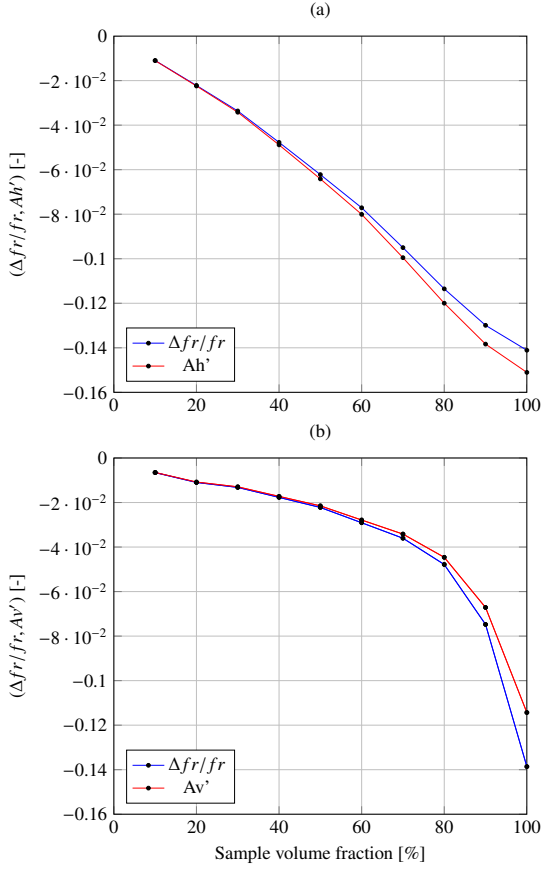
Figure 4: Perturbation analysis results based on experimental measurements for (a) horizontal and (b) vertical antennas placement.
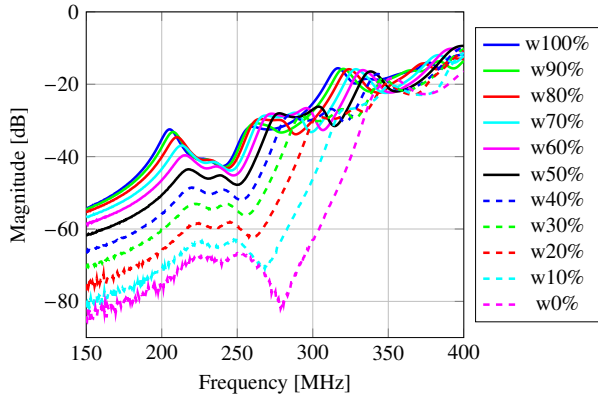
Figure 5: Magnitude of the transmission coefficient S_{21} according to frequency for each percentage of water fraction in a stratified water/air mixture (experimental results). Note that *w100%* means one hundred percent of water.
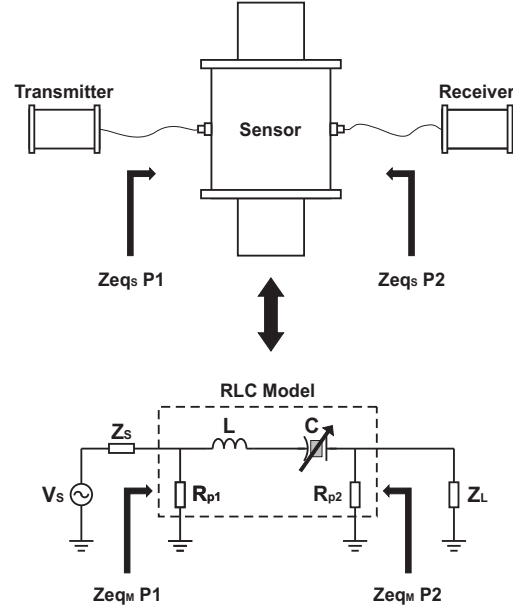
Figure 6: Lumped parameter model of the sensor.

3. Impedance matching analysis

3.1. Resonant cavity electrical model

Close to the resonance frequency, resonant cavities can be modeled as an equivalent resonant circuit with lumped components RLC [8], [20]. From the former assumption, the resonant cavity dynamic behavior for the first resonant mode was emulated through a series RLC circuit. In what follows, this RLC model will be considered to analyze the sensor behavior using a circuit simulation environment.

The RLC resonant circuit has a resonant frequency given by

$$f_0 = \frac{1}{2\pi \sqrt{LC}}. \tag{9}$$

From the relationship between the equations (2) and (9), the capacitance C can be expressed as a function of the relative permittivity ε_m, that varies according to the percentage of water in the mixture, as given by (10).

$$C = \frac{\varepsilon_m}{L} \left(\frac{1}{11,3846\, c\, \pi} \right)^2. \tag{10}$$

A resistor was added to the circuit model in parallel to each port ($Rp1$ and $Rp2$) in order to represent the losses generated by the port and metallic walls, as illustrated in Figure 6.

5
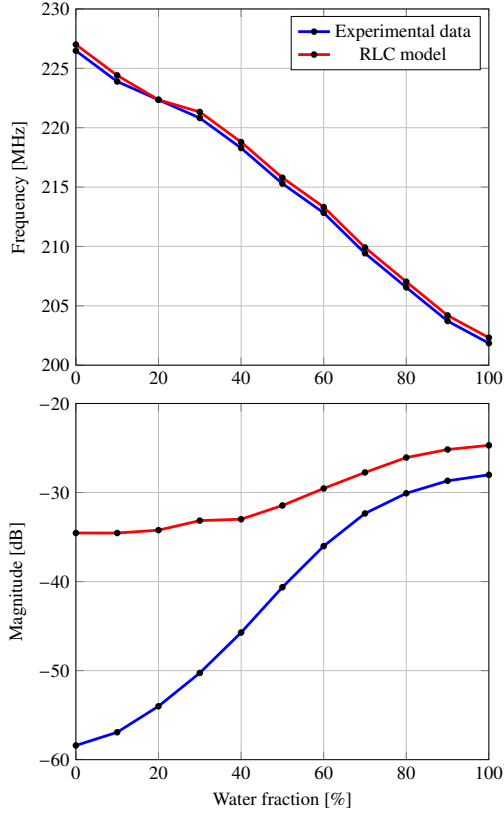
Figure 7: Resonance frequency (a) and signal magnitude of the transmission coefficient S_{21} (b) of the cavity as a function of the water fraction in a water/air mixture.

Figure 8: Example of an impedance matching design between a complex impedance source Z_S and a complex impedance load Z_L using L network design.

In this circuit, Z_S and Z_L are the impedances of the transmitter and receiver modules respectively, whose values of 50 Ω were obtained from the datasheet of these modules. The value of the inductor L was empirically determined as 80 nH. $Zeq_S P_1$ and $Zeq_S P_2$ are the equivalent impedance from experimental values of the port 1 and 2 of the sensor respectively, whereas $Zeq_M P_1$ and $Zeq_M P_2$ are the equivalent impedance of the port 1 and 2 of the RLC model respectively. The Rp_1 and Rp_2 values were found considering that $Zeq_S P_1 = Zeq_M P_1$ and $Zeq_S P_2 = Zeq_M P_2$.

All the measurements were performed taking into account a water/air variation in the pipe. A comparison between experimental data and RLC model results is shown in Figure 7. We can observe that the measured resonance frequency of the cavity correlates well with the resonance frequency of the model. The model is only accurate for the first resonance mode of the cavity. Extra sources of uncertainties, such as the purity of the fluids and errors on the volume of the water, were not taken into account.

We can also observe that the signal presents a large attenuation, specially at low water fractions, where the resonance peak almost disappears. Therefore, the quality factor is also reduced, so that the first resonance becomes more noisy and inappropriate to be used as a measurement parameter. The lower the quality factor, the more uncertainty occurs in the peak identification. The main reason for this behavior is the impedance mismatch between the transmitter and receiver modules (50 Ω) and the coupling probes from the sensor (approximately 1 to 2 Ω) in the operating frequency range (from 200 MHz to 230 MHz).

In what follows, we propose the adoption of an impedance matching network for improving the accuracy of the sensor.

3.2. Impedance matching design

The purpose of adding an impedance matching network is to improve the power transfer between source and load. This is a common technique in several applications, as for example in communication system, medical applications, and recently applications in wireless energy transfer [21], [12], [13], [22].

Most impedance matching networks are designed taking into account reactive loads. It is shown in Figure 8 the use of impedance matching between two different reactive loads. For maximum power transfer, the primary objective in any impedance matching scheme is to transform the load impedance in the complex conjugate of the source impedance. So, there are different techniques to accomplish it. One of the simplest technique is to add an L network between source and load, which consists of a combination of two reactive devices
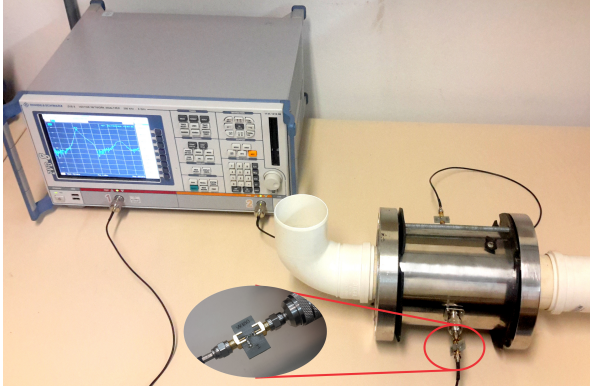
Figure 9: Setup implementation to extract the sensor's S-parameters for each percentage of water fraction using a Vector Network Analyzer (detail of the impedance matching network coupled at the sensor's port).

in a shunt-series or series-shunt configuration as shown in Figure 8. In Figure 8, the values of Xs and Xp are calculated as (considering that $R_S > R_L$) [23]:

$$Xs = QR_L \qquad (11)$$

$$Xp = \frac{R_S}{Q} \qquad (12)$$

where R_L and R_S are the resistances from the load and source respectively, and Q is the quality factor of the circuit.

In order to perform the impedance matching design we use a Vector Network Analyzer (VNA) to extract the magnitude and phase of S-parameters of the sensor for each percentage of water fraction. The setup implementation using the VNA is shown in Figure 9. In Figure 10 we can observe that the impedance of the sensor ports varies according to the water fraction proportion. The real part presents a variation between 1 Ω and 1.8 Ω whereas the imaginary part varies approximately between j8 Ω and j12 Ω. Therefore, there is a large impedance mismatch between the sensor ports and the transmitter/receiver modules, since the impedance of the transmitter and receiver is 50 Ω, as shown in Figure 11.

The L network designed is formed by three lumped elements, a source shunt capacitor Cp, a load series inductor Ls and a load series capacitor Cs. The load series capacitor Cs was used to reduce the inductive reactive part of the load in order to allow an Ls value greater than the previous calculated. Considering $Cs = 18pF$
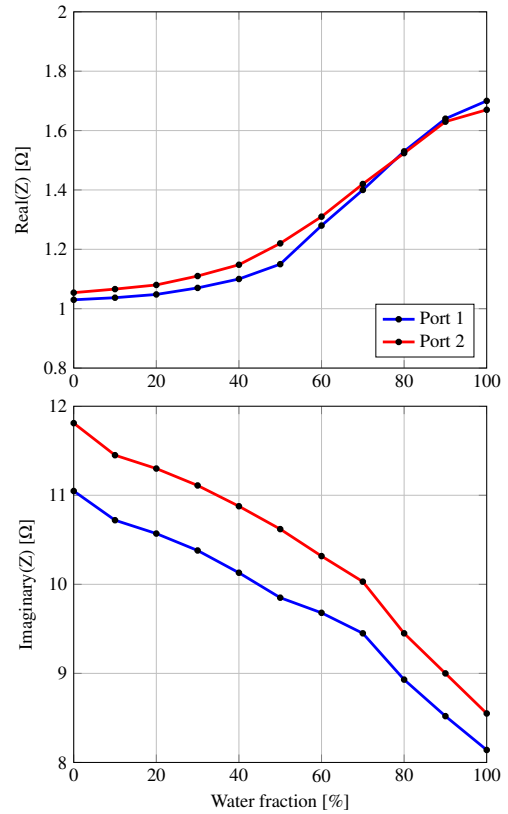
Figure 10: The dependence of resistance and reactance of the sensor's ports on water fraction at the resonance frequency (experimental values).
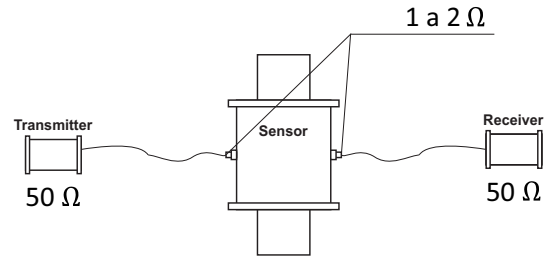
Figure 11: Impedance mismatch between the sensor ports and the transmitter/receiver modules.
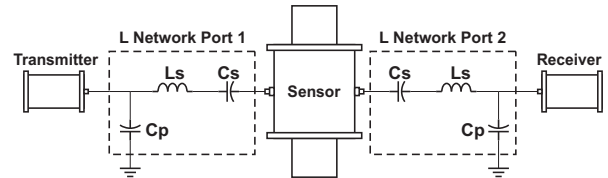
Figure 12: Schematic diagram of the sensor showing the impedance matching networks.

7

and using the equations (11) and (12) we can found the ideal values of the shunt element Cp and the series element Ls, taking into account the load impedance and resonant frequency for each percentage of water. We use an electromagnetic model of the circuit's layout in order to consider the parasitic impedance of the copper paths on the substrate. Finally we use real components with values near to the results obtained from the simulations. The values of the components are given in Table 1. A schematic diagram of the sensor showing the impedance matching networks is shown in Figure 12.

Table 1: Components values used in the implemented impedance matching networks.

Water fraction [%]	Cp [pF]	Ls [nH]	Cs [pF]
0	56	18	18
50	56	22	18
100	39	33	18

Simulation and experimental results obtained for the sensor with impedance matching networks are shown in Section 4.

4. Simulation and experimental results

All simulations were performed using the software Advanced Design System (ADS) from Agilent company. A comparison between the magnitude of transmission coefficient S_{21} at the resonant frequency according to the water fraction before and after the impedance matching network implementation is depicted in Figure 13. The curves in blue and in red color in Figure 13 correspond to the water-cut meter without and with the proposed impedance matching network, respectively. For the matching design the impedance and frequency values were considered for each percentage of water, being the impedance matching networks formed by ideal components. As we can observe in Figure 13, the results show about 18 dB gain at high water fractions and around 22 dB gain at low water fractions.

The transmission coefficient for each percentage of water with the matching networks simulated on ADS are shown in Figure 14 (cf. Figure 5). We can observe that the sensor with the impedance matching network reduces the attenuation between 150 MHz and 250 MHz for the first resonant mode and strongly attenuates the other resonant modes, such that only one maximum resonant peak is now available to be reliably detected.

Three impedance matching networks with fixed components considering the impedance and frequency values for 0%, 50% and 100% of water fraction were implemented. A picture of the implemented circuit proto-
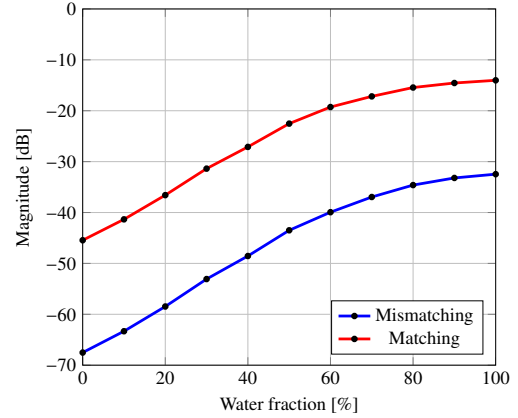
Figure 13: A comparison between the magnitude of transmission coefficient S_{21} at the resonant frequency according to the water fraction before and after the impedance matching network implementation (simulation results).
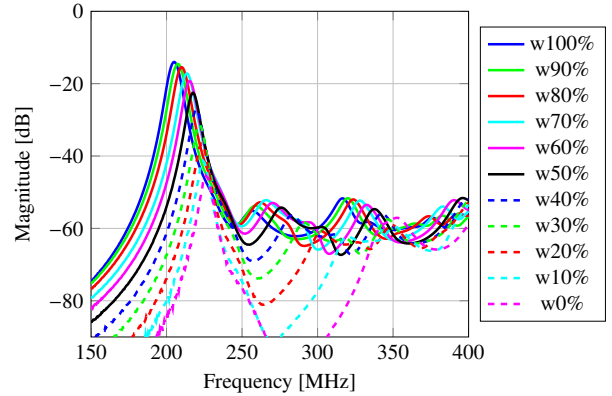
Figure 14: Magnitude of the transmission coefficient S_{21} according to frequency for each percentage of water fraction in a stratified water/air mixture after the impedance matching implementation (simulation results).

Figure 15: Impedance matching networks for 0%, 50% and 100% of water fractions.

types is shown in Figure 15. The simulated and experimental results of the magnitude of transmission coefficient with and without the impedance matching networks for 0%, 50% and 100% of water fraction are shown in Figures 16, 17 and 18 respectively. As we can see, the simulated and experimental results are very correlated, mainly for 100% of water fraction. A comparison between the Maximum Gain (MAG) expected and the results from the simulated and experimental measurements is given in Table 2.

Table 2: Comparison between the MAG and simulated/experimental results.

Water fraction [%]	MAG [dB]	Simulated results [dB]	Experimental results [dB]
0	-45.71	-48.98	-55.11
50	-30.40	-35.38	-39.93
100	-14.58	-21.75	-22.39

From Table 2, it can be highlighted that for all cases the experimental results are correlated with the simulation results, mainly for 100% of water. The difference between the experimental results and the MAG was about 9,4 dB, for 0% and 50% of water fraction, and 7,81 dB for 100% of water fraction case. These results show that there is approximately 4,7 dB attenuation in the transmission signal for each impedance matching network, designed for 0% and 50% of water fraction, and around 3,9 dB attenuation for those impedance matching networks designed for 100% of water fraction.

The reflection coefficient in each port with and without the impedance matching networks for 0%, 50% and 100% of water fraction are shown in Figures 19, 20 and 21 respectively. The markers represent the impedance at the resonance frequency before the matching implementation (circles), after matching implementation from the simulation results (stars) and after matching implementation from the experimental results (triangles). We can note that in the resonance frequency for 0% and 50% of water the real part of the impedance reaches around 30% and 40% of the expected value (center of the Smith Chart) respectively, with some reactive load, whereas for 100% of water the results are even better reaching around 90% of the expected value also with some reactive load.

One possible approach to improve the current results is to employing variable capacitors in order to have more degrees of freedom to adjust the parameters of the impedance matching circuits.
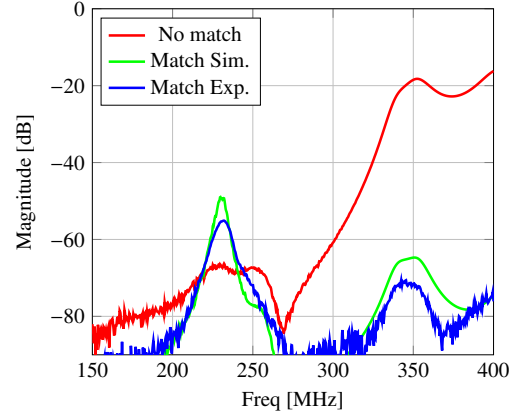
Figure 16: Magnitude of the transmission coefficient S_{21} for 0% of water fraction.
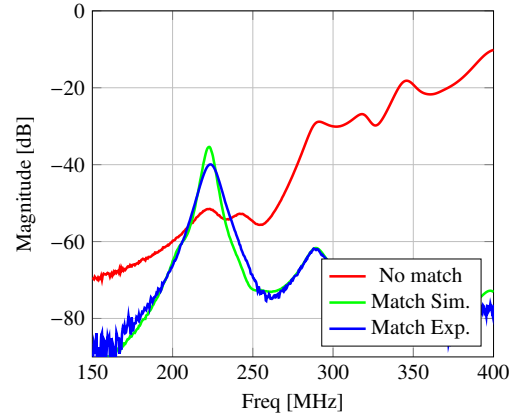
Figure 17: Magnitude of the transmission coefficient S_{21} for 50% of water fraction.
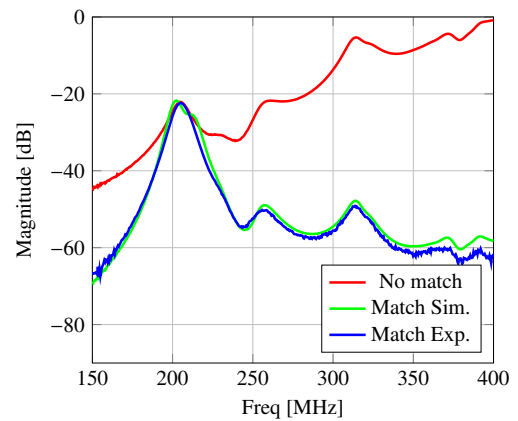
Figure 18: Magnitude of the transmission coefficient S_{21} for 100% of water fraction.

9
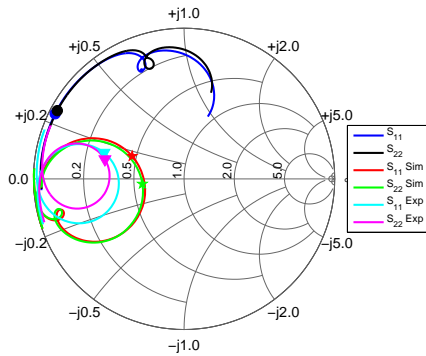
Figure 19: Impedance matching analysis for ports 1 and 2 in the Smith Chart for 0% of water.
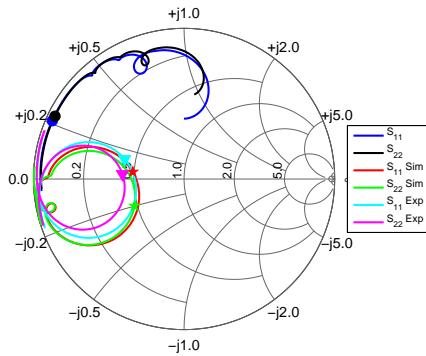
Figure 20: Impedance matching analysis for ports 1 and 2 in the Smith Chart for 50% of water.
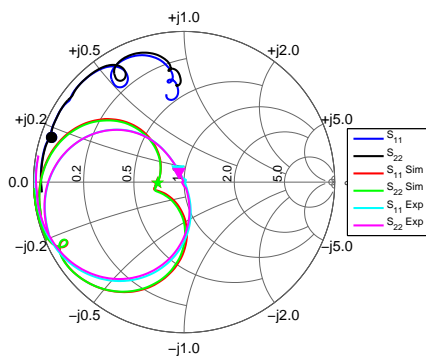
Figure 21: Impedance matching analysis for ports 1 and 2 in the Smith Chart for 100% of water.

5. Conclusion

The accuracy of electromagnetic water-cut meters, based on high RF cavity sensors, depends on the reliable detection of the first resonant peak of the transmission coefficient at the resonant frequency. The first resonant peak is affected by the content of water in the flow, so that the less water fraction, the more attenuated became the signal. Moreover, this attenuation phenomenon is amplified due to the impedance mismatch between the sensor ports and the transmitter/receiver modules. In order to solve this problem, several impedance matching networks based on lumped elements were simulated and three prototypes for 0%, 50% and 100% of water fractions were implemented to validate the impedance matching design.

The impedance matching approach proposed in this paper has improved the accuracy of the resonant peak identification and contributes to develop more reliable water-cut meters.

The proposed water-cut meter can be used in wellhead and subsea applications to measure water cut, mainly, in heavy oil applications where water and oil density are very close.

6. Acknowledgments

References

[1] Y. Li, W. Yang, Z. Wu, D. Tsamakis, C. Xie, S. Huang, C. Lenn, Gas/oil/water flow measurement by electrical capacitance tomography, in: IEEE International Conference on Imaging Systems and Techniques (IST), 2012, pp. 83–88.

[2] H.-J. Lim, K.-A. Chang, C. B. Su, C.-Y. Chen, Bubble velocity, diameter, and void fraction measurements in a multiphase flow using fiber optic reflectometer, Review of Scientific Instruments 79 (12).

[3] J. Carlson, A. Grennberg, Ultrasonic measurements of particle concentration in a multiphase flow, in: IEEE Proceedings of the Ultrasonics Symposium, Vol. 1, 1999, pp. 757–760.

[4] S. R. Wylie, A. Shaw, A. I. Al-Shamma'a, RF sensor for multiphase flow measurement through an oil pipeline, in: Measurement Science and Technology, Vol. 17, 2006, pp. 2141–2149.

[5] S. Al-Hajeri, S. R. Wylie, A. Shaw, A. I. Al-Shamma'a, Real time EM waves monitoring system for oil industry three phase flow measurement, in: Journal of Physics: Conference Series, Vol. 178, 2009, pp. 1–6.

[6] S. Al-Hajeri, S. R. Wylie, R. A. Stuart, A. I. Al-Shamma'a, An electromagnetic cavity sensor for multiphase measurement in the oil and gas industry, in: Journal of Physics: Conference Series, Vol. 76, 2007, pp. 1–6.

[7] M. Al-Kizwini, S. Wylie, D. Al-Khafaji, A. Al-Shamma, The monitoring of the two phase flow-annular flow type regime using microwave sensor technique, in: Measurement, Vol. 46, 2013, pp. 45–51.

[8] E. Nyfors, P. Vainikainen, Industrial Microwave Sensors, Artech House, Norwood, MA, 1989.

[9] Handbook of Multiphase Flow Metering, The Norwegian Society for Oil and Gas Measurement, Norwegian, 2005.

[10] J.-S. Cong, X.-M. Wang, D.-H. Chen, D.-L. Xu, C.-X. Che, S.-L. Ma, Gas detection in a gas-liquid flow using an acoustic resonance spectroscopy method, in: Chinese Journal of Geophysics, Vol. 51, 2008, pp. 191–196.

[11] R. A. Hatinoor, The effect of gas on microwave resonance frequency meter technology, Ph.D. thesis, Universitetet i Stavanger, Faculty of Science and Technology, Stavanger, Norway (2013).

[12] T. Yabuhara, K. Kato, K. Tsuchiya, T. Shigihara, T. Uzuka, H. Takahashi, Development of the re-entrant type resonant cavity applicator for brain tumor hyperthermia - experimental heating results, in: 28th Annual International Conference of the IEEE Engineering in Medicine and Biology Society, EMBS 06, 2006, pp. 5161–5164.

[13] S. Cheon, Y.-H. Kim, S.-Y. Kang, M.-L. Lee, J.-M. Lee, T. Zyung, Circuit-model-based analysis of a wireless energy-transfer system via coupled magnetic resonances, in: IEEE Transactions on Industrial Electronics, Vol. 58, 2011, pp. 2906–2914.

[14] Y.-K. Jung, B. Lee, Design of adaptive optimal load circuit for maximum wireless power transfer efficiency, in: Asia-Pacific Microwave Conference Proceedings (APMC), 2013, pp. 1221–1223.

[15] H. Jiang, J. M. Zhang, S. S. Liou, R. Fechter, S. Hirose, M. Harrison, S. Roy, A high-power versatile wireless power transfer for biomedical implants, in: Annual International Conference of the IEEE Engineering in Medicine and Biology Society (EMBC), 2010, pp. 6437–6440.

[16] R. A. Waldron, Perturbation theory of resonant cavities, The Institute of Electrical Engineers (373).

[17] R. F. Harrington, Time-Harmonic Electromagnetic Fields, McGraw-Hill, New York, 1961.

[18] L. F. Chen, C. K. Ong, C. P. Neo, V. V. Varadan, V. K. Varadan, Microwave Electronics: Measurement and Materials Characterization, John Wiley & Sons, Ltd, England, 2004.

[19] A. Sihvola, Electromagnetic mixing formulas and applications, The Institution of Engineering and Technology, London, UK, 2008.

[20] D. M. Pozar, Microwave Egnineering, John Wiley & Sons, Inc., Danver, MA, 2005.

[21] V. Iyer, S. Makarov, D. Harty, F. Nekoogar, R. Ludwig, A lumped circuit for wideband impedance matching of a non-resonant, short dipole or monopole antenna, in: IEEE Transactions on Antennas and Propagation, Vol. 58, 2010.

[22] H.-S. Kim, D.-H. Won, B.-J. Jang, Simple design method of wireless power transfer system using 13.56 mhz loop antennas, in: IEEE International Symposium on Industrial Electronics (ISIE), 2010.

[23] C. Bowick, Electromagnetic mixing formulas and applications, RF Circuit Design, Burlington, USA, 2008.